LARGE-EDDY SIMULATION OF NON-CIRCULAR JET FLOW IN A PILOT-SCALE INLINE HIGH-SHEAR STATIC MIXER

V. Michael[1], *I. Bagkeris*[1], *U. Ahmed*[2], *R. Prosser*[1] *and A. Kowalski*[3]

[1] *School of Mechanical, Aerospace & Civil Engineering, University of Manchester, Manchester, M13 9PL*
[2] *School of Engineering, Newcastle University, Newcastle upon Tyne, NE1 7RU*
[3] *Unilever R&D, Port Sunlight Laboratory, Quarry Road East, Bebington, Wirral CH63 3JW*

vipin.michael@manchester.ac.uk

Abstract

This paper examines the flow characteristics of a pilot-scale high shear mixer using Large Eddy Simulation (LES). The mixer consists of a non-planar elliptic jet released into a confined cylindrical chamber. The simulated results are validated by comparing mean quantities with published PIV data. Fundamental turbulence quantities including turbulent kinetic energy, turbulence production and dissipation, Reynolds stress anisotropy and triple moments of velocity are examined. The orifice produces asymmetric shear layer evolution, spreading and turbulence intensities between the major and minor axes planes. Jet entrainment and turbulence activity in the near-field is promoted when compared to other non-circular planar jets from literature. The turbulence field exhibits similar anisotropy to the mean flow. Implications of the results for droplet breakup modelling are also discussed in this paper.

1 Introduction

High shear static mixers are widely used in the process industry for the manufacture of emulsion based personal care products as they are able to deliver localised high shear and turbulent energy densities which accelerates mixing and dispersion of liquid-liquid systems. The properties of these formulated emulsions are process sensitive, with droplet size affecting the physical stability and consumer appeal of the final product. Drop dispersion and breakage is predicated on the turbulence characteristics of the continuous phase.

Traditional droplet breakup modelling in turbulent flows is based on the assumption of isotropic turbulence of infinite Reynolds number which is inconsistent in practical flows of industrial interest. This results in the use of empirical models and system-specific parameter fitting based on experimental results to arrive at predictive correlations. To improve drop breakup modelling and obtain reliable correlations a sound investigation of the underlying flow dynamics and turbulence characteristics of actual mixer configurations at representative operating conditions is required.

A pilot-scale model of a Sonic Corporation mixer is simulated using LES in this study. PIV results from the experimental investigation of Ryan et al (2017) is used to validate the numerical results. This work formed part of a recently concluded project which aimed to reduced reliance on physical prototype testing by promoting in-silico evaluation of manufacturing concepts.

2 Methodology

The mixing element of this device comprises of a V-shaped notch cut at 60^o through a hemispheric closed ended tube to form a horizontal cats-eye shaped orifice. The mixer operates by forcing fluid under high pressure through the orifice, with the ensuing high velocity jet exiting into a confined cylindrical chamber (Figure 1). Due to initial disagreements between the pressure drop measurements of Ryan et al (2017) and CFD results, a laser microscope was used to measure the diameters of the physical orifice and produce a 2-D projection of the area. The CFD geometry was then adjusted matching the measured area and the diameters of the ellipse. A structured mesh of the computational domain was produced using two O-grids. This meshing strategy ensured capturing the complex geometry of the elliptic orifice and the V-shaped cut without introducing excessive cell distortion.

The working fluid is water and the mass inflow rates of the simulations were $0.046-0.092$ kg/s to match Ryan et al (2017) and remain below the onset of cavitation. Near-wall resolution on the orifice nozzle of $0.1<Y^+<6$, $27<\Delta X^+<9$ and $12<\Delta Z^+<50$ were used. The numerical simulations were performed using Code_Saturne (Archambeau et al (2004)). The Dynamic Smagorinsky model (Germano et al (1991) is used to model the sub-grid scale (SGS) stresses. A 2^{nd} order centred scheme is used for space and time discretisation. Inflow turbulence is prescribed using the synthetic eddy method (Jarrin et al (2002)). Target statistics for the synthetic turbulence is prescribed through a precursor periodic pipe flow calculation using EBRSM (Manceau and Hanjalic (2002)) to pro-

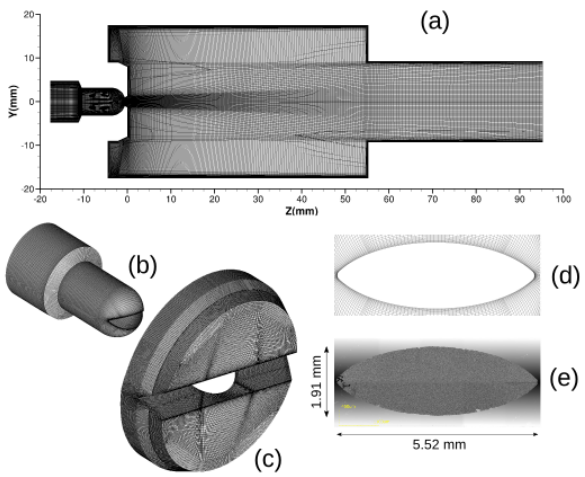

Figure 1: Computational mesh: (a) cross-section of volume mesh in the plane parallel to the orifice small diameter, (b) surface mesh of the inlet chamber, (c) surface mesh of the orifice from the side of the main chamber, (d) close-up view of the orifice surface mesh, (e) orifice image captured with laser microscope and and dimensions of the major and minor diameters (measured orifice area A_e=7.68mm^2 and aspect ratio AR=2.89).

duce a fully-developed turbulent profile (H=1.4315, mean $T.I.$=9.2%).

The fidelity of the simulation can be observed from the resolved spectra of streamwise velocity along the centreline and in the shear layer shown in Figure 2. The figure shows that the inertial subrange and larger scales are adequately captured.

3 Results

Results in this section are presented for a jet orifice Reynolds number Re=37,000. Simulations were also run at Re=18,500 and qualitatively similar results were obtained. The reference length and velocity scales were taken as the nominal orifice diameter D=$\sqrt{A_e}$=2.7mm and bulk mean velocity at the orifice W_b=$\frac{1}{A_e}\int W dA$=12.9m/s unless indicated otherwise. Comparison of mean velocity between the simulation and PIV results are given in Figures 3 and 4 and show reasonably good agreement. Excellent agreement of pressure drop across the mixer with PIV ($\sim$ 4%) was also found.

Boundary layer characteristics at the jet exit indicate a laminar profile (H=2.344 and $T.I.$=1.76%). The non-circular nature of the orifice produces differential evolution of the jet shear layers in the major and minor axis planes. The mean shear layers are depicted using mean vorticity contours in Figure 5 demonstrating wider jet diameter and slow monotonic spreading in the major axis plane as compared to the minor axis plane. The figure also depicts the half-velocity widths to indicate the extent of jet spreading in each plane.

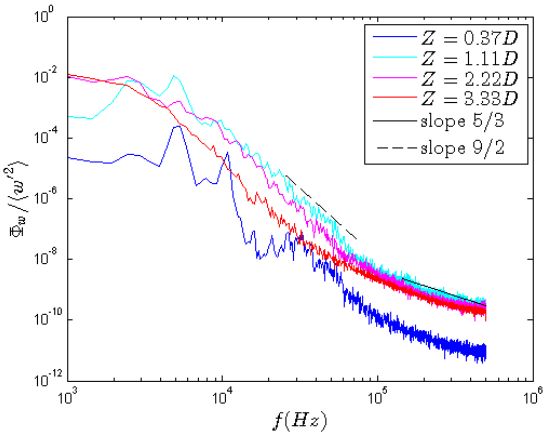

(a) Centreline. The slopes indicate the inertial and energy containing subranges.

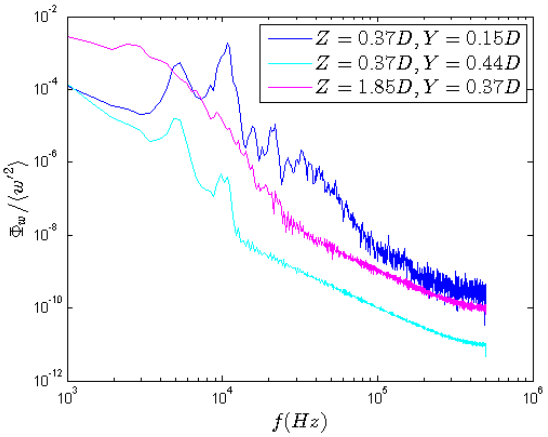

(b) Shear layer

Figure 2: Power spectral density (Φ_w) of streamwise velocity w

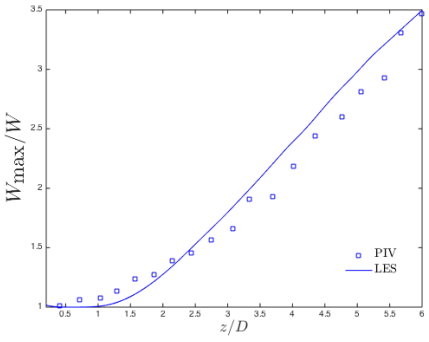

Figure 3: Comparison of streamwise mean velocity profiles between CFD and PIV. W_{max} is the maximum of the centreline velocity. Centreline decay of the jet is shown. The LES data is used to calculate the potential core length and decay rate

The streamwise evolution of the jet cross-section (Figure 6) reveals an initial two-lobed shape leading to flatter and wider cross-section downstream due to greater jet spreading along the major axis. The jet

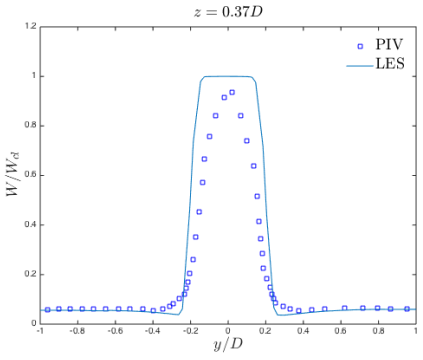

(a) $z = 0.37D$

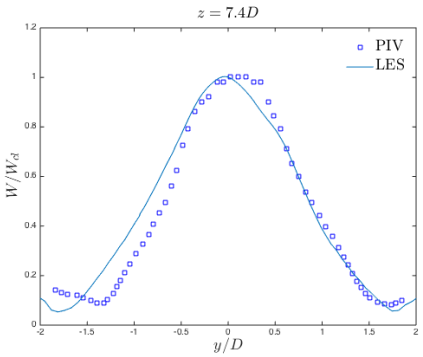

(b) $z = 7.4D$

Figure 4: Profiles of streamwise mean velocity profiles on the minor axis at two different streamwise locations from CFD and PIV. W_{cl} is the streamwise velocity on the centreline.

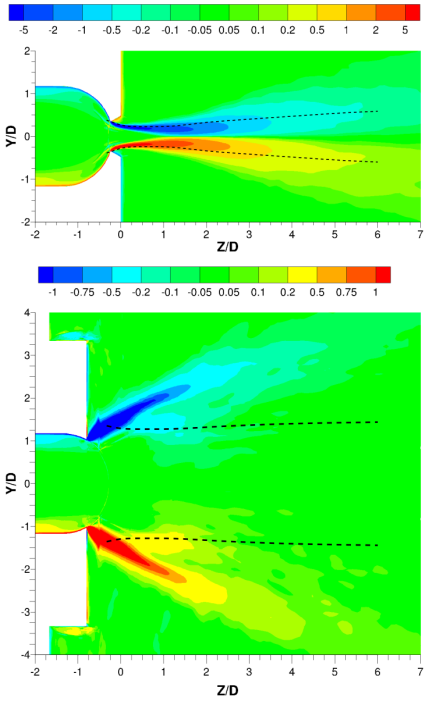

Figure 5: Normalised mean vorticity (spanwise to plane) contours with jet half-widths super-imposed as dotted lines on minor axis (top) and major axis (bottom) planes.

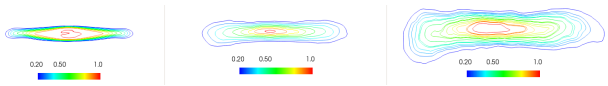

Figure 6: Streamwise evolution of jet cross-sectional shape depicted using contours lines of W/W_{cl}.

cross-sectional shape thus follows the orifice contour without any switching of the ellipse axes. The absence of axis-switching potentially limits far-field jet entrainment and mixing.

The jet decay rate is calculated as 0.578 and potential core length is $1.2D$ indicating faster decay and greater near-field entrainment compared to values reported for elliptic planar jets (Mi and Nathan (2010), Aleyasin et al (2017)). The jet spreading rate, calculated using the equivalent half-widths (geometric mean of the respective values in each plane), is 0.063 and is smaller than those reported in the above studies.

Analysis of the instantaneous flow-field (Figures 7 and 8) reveals vortex shedding due to shear layer separation at the orifice lips, and downstream formation of larger scale coherent structures. In the near field, roll-up of shear layer at orifice produces spanwise line vortices that deform as they convect downstream due to Biot-Savart induced velocities (see Figure 9 showing iso-surfaces of Q, the second invariant of the velocity gradient tensor). The streamwise velocity spectra in the centreline (Figure 2a) and shear layer (Figure 2b) reveal that the dominant frequencies for the jet preferred mode and shear layer mode instabilities are comparable. Strouhal numbers (St_D=0.82 and St_θ=0.027 based on orifice diameter and jet exit momentum thickness respectively) are comparable to values for round and planar elliptic jets (Sadeghi and Pollard (2012), Mi and Nathan (2010). With downstream evolution the peaks shift to near subharmonics of the main mode indicating interaction of vortices. The interaction between the spanwise line vortices in the shear layer and the braid (rib) vortices in the jet core form streamwise hairpin vortices that eventually breakdown into smaller scale structures downstream.

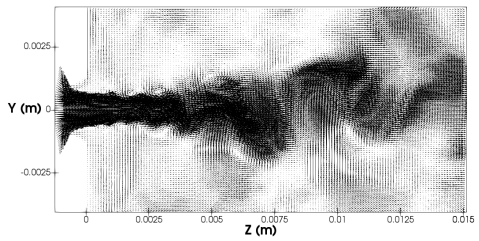

Figure 7: Instantaneous velocity vectors in the minor axis plane.

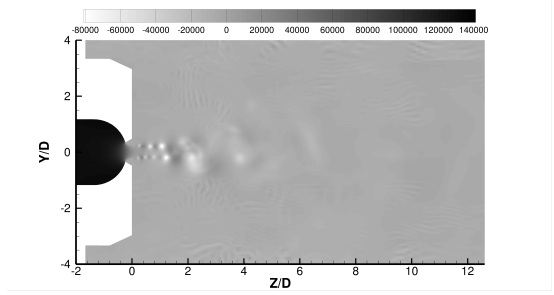

Figure 8: Pressure contours depicting vortex shedding in minor axis plane.

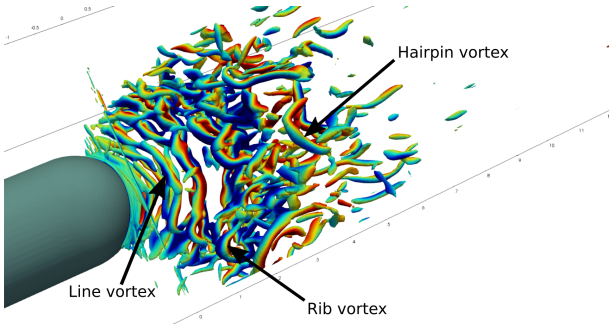

Figure 9: Q iso-surfaces coloured by transverse velocity depicting line and rib vortices after the jet exit and hairpin vortices downstream.

The turbulence characteristics of the flow-field are investigated. The regions of large TKE (Figure 10) and dissipation rate (Figure 11) occur within the shear layer after the potential core. Peak TKE production (Figure 12) occurs at the edges of the shear layer surrounding the potential core. Production is negative immediately after the jet exit leading to the growth of larger vortices. A similar result has also been reported in 3-D planar jets (Bisoi et al (2017)). The locations of maximum TKE and dissipation rate are relatively upstream compared to other non-circular planar jets (Aleyasin et al (2017)). Regions of intense turbulent activity is confined between $2-4$ orifice diameters downstream of the jet exit which is beneficial for promoting droplet breakup in the jet near-field. Asymmetric evolution of the mean shear layer results in similar asymmetric pattern in the turbulence field. A more homogenous turbulence field would potentially favour uniform droplet breakup rates in the flow-field resulting in narrower distribution of drop-sizes.

The distribution of the components of the Reynolds stresses are shown in Figure 13. For brevity the discussion is restricted to the minor axis plane. The normal components are indicative of the intensity of the large-scale fluctuations while the shear components are indicative of the momentum exchange between the jet and ambient fluid. The stresses are relatively low in potential core region but peak within the shear layers ($\sim 2-3$ diameters downstream) as the jet evolves. Streamwise fluctuations originate at the orifice lips due

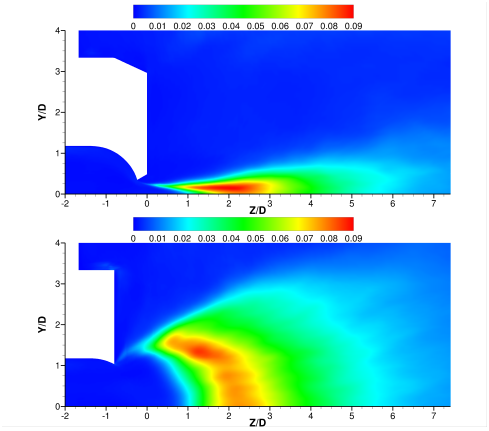

Figure 10: Normalised TKE contours in minor (top) and major (bottom) axis planes (half-planes shown due to symmetry).

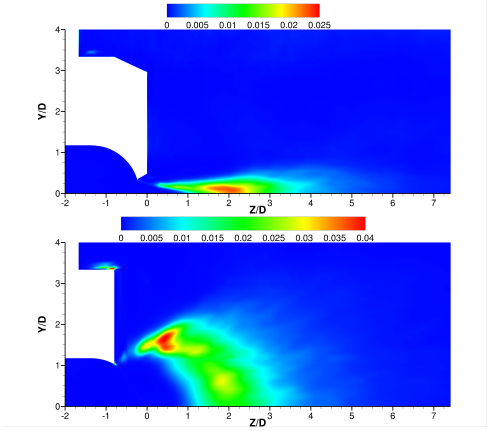

Figure 11: Normalised TKE dissipation rate contours in minor (top) and major (bottom) axis planes (half-planes shown due to symmetry).

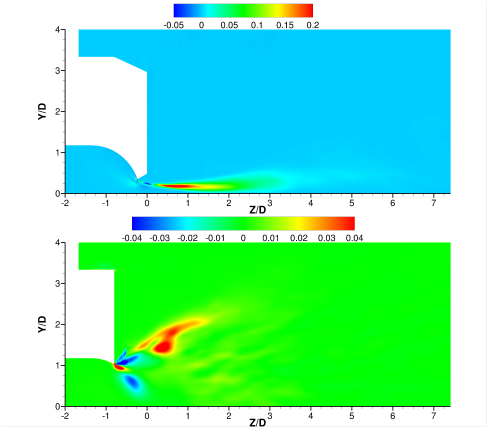

Figure 12: Normalised TKE production contours in minor (top) and major (bottom) axis planes (half-planes shown due to symmetry).

to vortex shedding. The transverse fluctuations are dominant in the core of the jet where vortex interaction is greatest. Spanwise fluctuations and shear stress are mainly driven by the shear layer downstream of the

exit plane of the orifice.

Profiles of the stress components along the minor axis (Figure 14) indicate that the normal stresses roughly exhibit self-similarity. Peak values of the shear stresses shift away from the centreline with downstream distance. The Reynolds stresses tend towards an axisymmetric state ($\overline{w'w'} \sim \overline{v'v'}$, $\overline{v'w'} \sim \overline{u'u'}$) outside the shear layer.

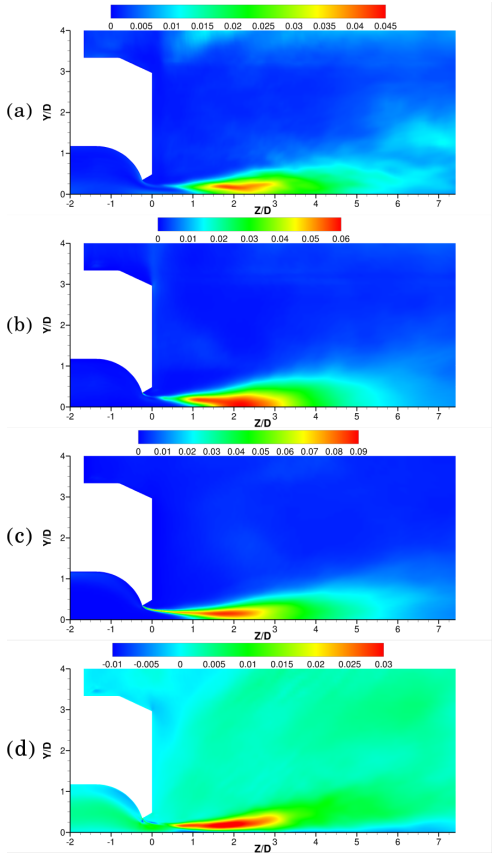

Figure 13: Reynolds stresses components in the minor axis plane: (a) $\overline{u'u'}/W_b^2$, (b) $\overline{v'v'}/W_b^2$, (c) $\overline{w'w'}/W_b^2$, (d) $\overline{v'w'}/W_b^2$ (half-plane shown due to symmetry, $\overline{v'w'}/W_b^2 < 0$ in the lower-half plane).

Plotting the invariants of the Reynolds stress anisotropy tensor on the Lumley triangle (Figure 15) shows that the most common shape of the Reynolds stresses is an prolate spheroid (ξ>0), which implies that the Reynolds stresses are in an axisymmetric extensive state and are representative of the Reynolds stresses found in boundary layer type flows (Pope 2000).

Diffusive transport of turbulence is represented by the gradients of the triple moments of the velocity. Figure 16 represents the profiles of the moments of TKE and shear stresses with the transverse velocity fluctuation. The negative gradient of the shear moments within the shear layer indicate diffusion of turbulent shear towards the centreline. The gradients of the normal moments on the other hand first become positive and then negative indicating diffusion of TKE

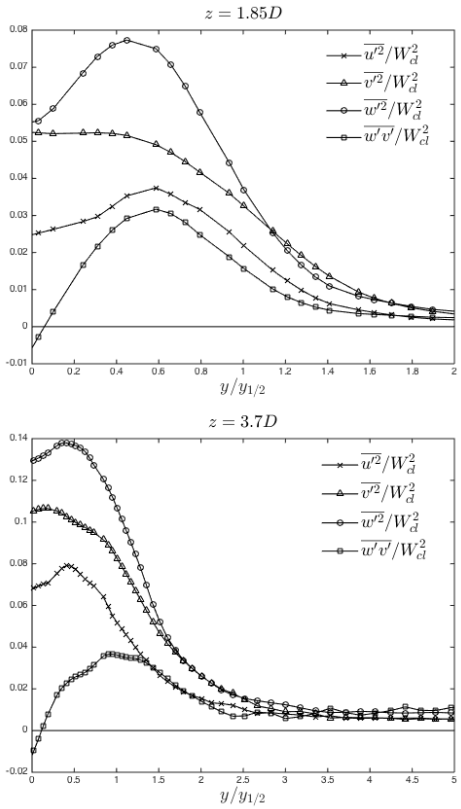

Figure 14: Variation of Reynolds stresses in the minor axis plane at two streamwise locations (only half profile is depicted due to symmetry).

away from the core and ambient toward the shear layers.

4 Conclusions

This paper describes a Large-Eddy Simulation of the flow in a pilot scale industrial high-shear static mixer used for emulsification applications. The flow features described are specific to the particular geometric configuration of the mixer. The flow in this configuration results in shorter potential core, smaller spreading rate and suppression of axis switching when compared to elliptic planar free jets. The orifice shape promotes entrainment and vortex interaction in the near-field. Diffusion of turbulence stresses by the fluctuating velocity field concentrates turbulent kinetic energy and shear stresses within the jet shear layers. The flow configuration is effective in delivering regions of localised turbulent energy dissipation that drive droplet breakup in the minor axis plane as compared to the major axis. The regions of peak turbulent energy dissipation coincide with the region of jet decay and intense vortex interactions.

The energy spectrum of the turbulence cascade was calculated and is of importance for improving drop breakage modelling in non-isotropic turbulence conditions (Bagkeris et al. (2018)). The traditional approach assumes infinite Reynolds number and velocity

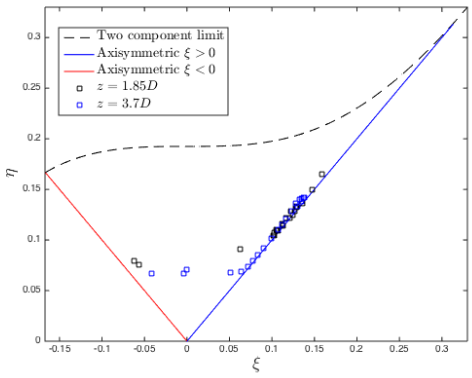

Figure 15: The Lumley triangle on the plane of the invariants ξ and η of the Reynolds stress anisotropy tensor (as defined in Pope (2000)). The data points correspond to locations along the minor axis at $z = 1.85D$ and $z = 3.95D$.

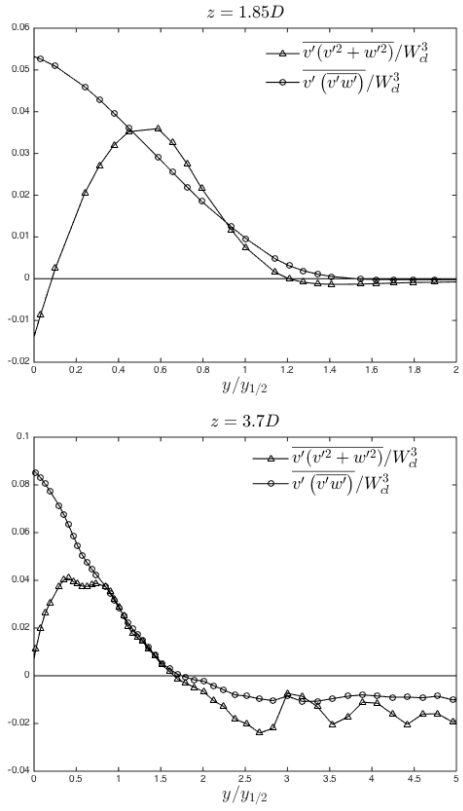

Figure 16: Transport of in-plane components of TKE and turbulent shear stress by transverse fluctuating velocity (only half profile is depicted due to symmetry).

scaling based on Kolmogorov's second order longitudinal structure function in the inertial subrange. The work of Solsvik et al. (2016) has extended this concept to finite Reynolds numbers using models for the entire energy spectrum of isotropic turbulence. The extent of the energy-containing subrange of the turbulent energy cascade (slope $-9/2$ in Figure 2a) and the spectral peaks corresponding to coherent structures in the jet near-field are of importance here, as the structure functions corresponding to the energy spectra in Figure 2 yield a velocity scaling notably different than both the traditional approach of drop breakage modelling and its extension to the entire spectrum of isotropic turbulence.

Acknowledgments

The authors would like to acknowledge funding from the UKRI and Unilever R&D, the assistance of Dr. Marc Schmidt and Prof. Mark Simmons and STFC UK Hartree Centre for computational time.

References

Archambeau F, Mchitoua N, Sakiz M. (2004) Code_Saturne: a Finite Volume Code for the Computation of Turbulent Incompressible Flows, *IJFV,* Vol. 1, pp 1-62.

Aleyasin, S., Tachie, M. and Koupriyanov, M. (2017), PIV Measurements in the Near and Intermediate Field Regions of Jets Issuing from Eight Different Nozzle Geometries, *FTAC,* Vol. 99, pp 329-351.

Bagkeris, I., Michael, V., Prosser, R., and Kowalski, A. (2018), Proceedings of the 16th European Conference on Mixing.

Bisoi, M., Das, M., Roy, S. and Patel, D. (2017), *Eur. J. Mech.-B/Fluids,* Vol. 65, pp. 423-429.

Germano, M., Piomelli, U., Moin, P. and Cabot, W. H. (1991), A Dynamic Subgrid-Scale Eddy Viscosity Model, *POF A*, Vol. 3, No. 7, pp. 1760-1765.

Jarrin, N. Benhamadouche S., Laurence, D. Prosser, R. (2006), A synthetic-eddy-method for generating inflow conditions for large-eddy simulations *IJHF,* Vol. 27, pp 585-593.

Manceau, R. and Hanjali?c , K. (2002), Elliptic blending model: a new near-wall Reynolds stress turbulence closure. *POF,* Vol. 14, pp 744?754.

Mi, J., Nathan, G. (2010), Statistical Properties of Turbulent Free Jets Issuing from Nine Differently-Shaped Nozzles, *FTAC,* Vol. 84, pp. 583-606.

Pope, S. (2000) Turbulent Flows. Cambridge University Press pp. 393-395.

Ryan, D., Simmons and M., Baker, M. (2017), Determination of the flow field inside a Sonolator liquid whistle using PIV and CFD, *Chem. Eng. Sci.* Vol. 163, pp. 123-136.

Sadeghi, H. and Pollard, A. (2012), Effects of passive control rings positioned in the shear layer and potential core of a turbulent round jet, *Physics of Fluids,* Vol. 24, pp. 115103-1-115103-22.

Solsvik, J., Skjervold, V.T., Han, L., Luo, H. and Jakobsen, H.A. (2016), A theoretical study on drop breakup modeling in turbulent flows: The inertial subrange versus the entire spectrum of isotropic turbulence, *Chem. Eng. Sci.*, Vol. 149, pp. 249-265.